Morphology Response to Strain Field Interferences in Stacks of Highly Ordered Quantum Dot Arrays

H. Heidemeyer,* U. Denker, C. Müller, and O. G. Schmidt

Max-Planck-Institut für Festkörperforschung, Heisenbergstrasse 1, D-70569 Stuttgart, Germany

(Received 10 July 2003; published 3 November 2003)

Twofold stacked InGaAs/GaAs quantum dot (QD) layers are grown on GaAs(001) substrates patterned with square arrays of shallow holes. We study the surface morphology of the second InGaAs QD layer as a function of pattern periodicity. Comparing our experimental results with a realistic simulation of the strain energy density E_{str} distribution, we find that the second InGaAs QD layer sensitively responds to the lateral strain-field interferences generated by the buried periodic QD array. This response includes the well-known formation of vertically aligned QDs but also the occurrence of QDs on satellite strain energy density minima. Our calculations show that base size and shape as well as lateral orientation of both QD types are predefined by the E_{str} distribution on the underlying surface.

DOI: 10.1103/PhysRevLett.91.196103 PACS numbers: 68.65.Hb, 81.07.Ta, 81.15.Hi

A vertical alignment of closely stacked self-assembled quantum dots (QDs) has been observed in many different material systems and relies on a strain-field interaction between a buried and a stacked quantum dot [1–6]. The buried QD generates a strain field, which reproduces the QD position in subsequent layers. For laterally periodic quantum dot arrays the strain fields of individual quantum dots have recently been predicted to interfere and produce satellite strain energy density minima on the surface [7]. However, a direct experimental observation of such interference has not been reported so far, since the fabrication of laterally strictly aligned QD arrays on planar surfaces with well-controllable periodicities is difficult to achieve [8–10]. In this Letter we fabricate highly ordered arrays of InGaAs/GaAs QDs on patterned substrates with different periodicities. We observe that a closely stacked InGaAs layer directly probes the strain-field interferences of the buried layer, forming vertically aligned QDs and QDs on satellite strain energy density minima. We show that the lateral position of the satellite QDs are caused by the elastic anisotropy of the GaAs host lattice.

We have grown 11.3 monolayers (ML) of $In_{0.3}Ga_{0.7}As$ followed by 8 nm GaAs, 3 nm $Al_{0.5}Ga_{0.5}As$, 2 nm GaAs, and 12 ML $In_{0.3}Ga_{0.7}As$. For a single InGaAs layer directly grown onto a square hole pattern, we recently reported the formation of a regular array of two closely spaced InGaAs QDs, which we termed lateral QD molecules (QDMs) [11]. For our sample, a GaAs buffer grown by molecular beam epitaxy (MBE) on a GaAs(001) substrate was patterned with 200 nm high and 500×500 μm^2 wide mesas using standard optical lithography and wet chemical etching. These large mesas served as markers in order to find the patterned areas for subsequent characterization. Square arrays of nanometer sized holes were defined on the large mesas by standard electron-beam lithography and reactive ion etching using $SiCl_4$. Exactly one square hole array (100×100 μm^2 area) was positioned in the center of each mesa. Several hole arrays with hole depths of 29 nm and different periodicities and diameters were fabricated and overgrown on one sample at the same time. After patterning, the sample was wet chemically cleaned and inserted into the MBE chamber. Prior to growth, the sample was irradiated with atomic hydrogen to remove residual remains of resist and native oxides [12]. The sample was directly overgrown at a substrate temperature of 500 °C. The final structures were investigated by atomic force microscopy (AFM) in tapping mode.

Figure 1 shows the surface morphology of a twofold stack of such InGaAs QD layers grown on square hole patterns with different periodicities. The QD array in Fig. 1(a) has a periodicity of 103 nm, identical with the initial periodicity of the hole array, and shows that a perfect site control of vertically aligned QDs can be achieved. As the periodicity increases to 157 nm [Fig. 1(b)], we still observe perfectly site-controlled QDs, but, additionally, several elongated structures occur between two nearest neighbor QDs in the [100] and [010] directions, which we denote in the following as satellite QDs. If we increase the periodicity to 179 nm [Fig. 1(c)] and 200 nm [Fig. 1(d)], increasingly more satellite QDs form on the surface, because the density of prepatterned sites reduces while the deposited amount of material remains the same.

The AFM images of Fig. 1 imply that the positions of the satellite QDs are not random but instead obey a lateral ordering mechanism. Figure 1(e) shows a position analysis of the formed QDs. The average number of vertically aligned QDs per prepatterned site is 1 and does not change, because we achieved perfect site control for all periodicities. The number of satellite QDs per prepatterned site increases with increasing periodicity from 4.2×10^{-4} to 0.68. At the same time, the average number

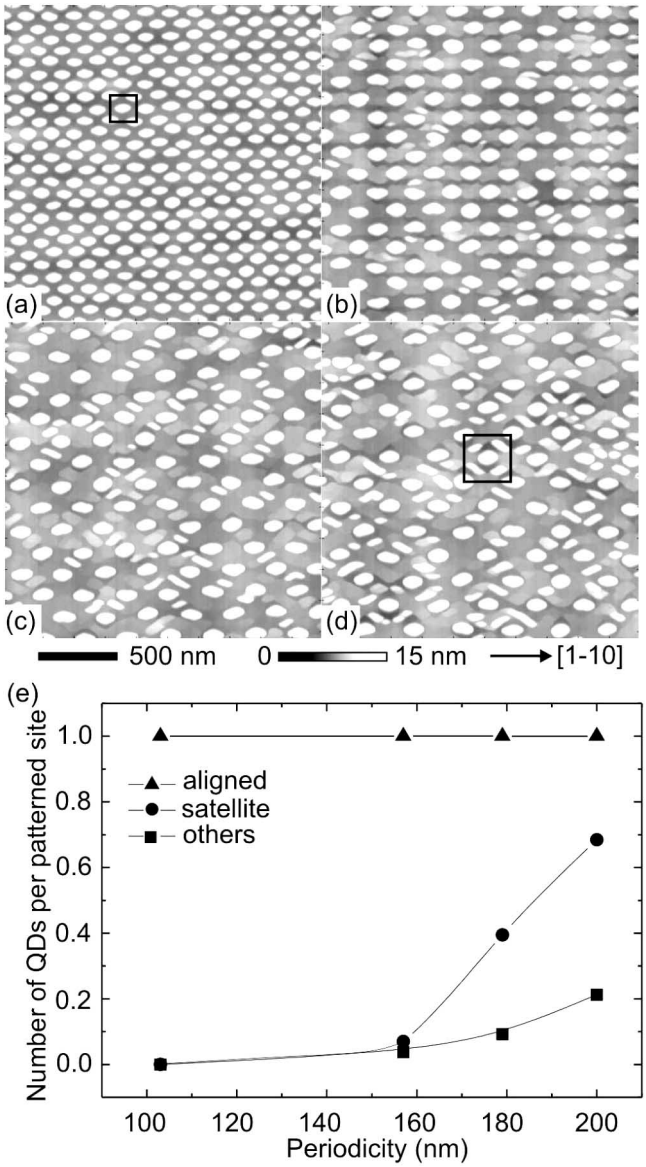

FIG. 1. InGaAs QDs grown on square hole patterns with (a) 103 nm, (b) 157 nm, (c) 179 nm and (d) 200 nm periodicity, overgrown with a twofold stack of InGaAs QDs. With increasing periodicity, the number of elongated structures between two neighboring QDs increases. The square areas, indicated in (a) and (d), are magnified in Figs. 4(b) and 4(d). (e) The average number per prepatterned site of aligned QDs, satellite QDs, and QDs on other sites as a function of periodicity.

of QDs forming on other positions increases only from 0 to 0.21. This analysis shows, that the satellite position is more likely to be occupied than others.

It is well known that the crystal anisotropy plays an important role in the vertical and lateral alignment of stacked QD layers [13]. Therefore, to understand the morphology of the second InGaAs layer, we calculate the strain energy density (E_{str}) distribution on the GaAs surface on top of the buried initial InGaAs QDM array. In our calculation we follow Ref. [14] taking the elastic anisotropy of the cubic GaAs crystal into account. The geometry of the buried QDM structure is derived from AFM images of a single InGaAs layer as shown in the inset of Fig. 2(a). The average height of each lens shaped QD is 4.5 nm and the diameter is 66 nm. Two of these QDs on top of the hole form the upper part of a QDM with a mean center to center distance of 66 nm. The diameter of a hole prior to growth is 54 nm and the depth is 29 nm. The material in the hole as well as in the QDs is assumed to be $In_{0.3}Ga_{0.7}As$.

To calculate the E_{str} distribution for an array of QDMs, the strain components ϵ_{ij} from all individual QDMs within the ordered array are superimposed. The ϵ_{ij} are then renormalized from the GaAs to the InAs lattice and the strain energy density is calculated by [15]

$$E_{\mathrm{str}} = \frac{c_{11}}{2}(\epsilon_{11}^2 + \epsilon_{22}^2) + c_{12}\epsilon_{11}\epsilon_{22} + 2c_{44}\epsilon_{12}^2$$

with $c_{11} = 83.4$ GPa, $c_{22} = 45.4$ GPa, and $c_{44} = 39.5$ GPa as elastic constants [16]. The z components are neglected, because we treat the growth plane as a free surface, which is relaxed in the z direction. Figure 2(a) shows a cross-sectional view of the E_{str} distribution through the middle of a single QDM (gray area). Areas with main E_{str} minima directly above and below the QDM can be identified, whereas areas with high E_{str} can be found around the molecule. The horizontal line 13 nm above the QDM indicates the GaAs surface, onto which the second InGaAs QD layer is grown. The lateral E_{str} distribution on this surface is given in Fig. 2(b). The E_{str} minima of the individual QDs and the hole have merged into one minimum, which is elongated in the $[1\bar{1}0]$ direction. Elongated E_{str} maxima are found next to the main minimum, pointing into the [110] and $[1\bar{1}0]$ directions. An important observation is the occurrence of

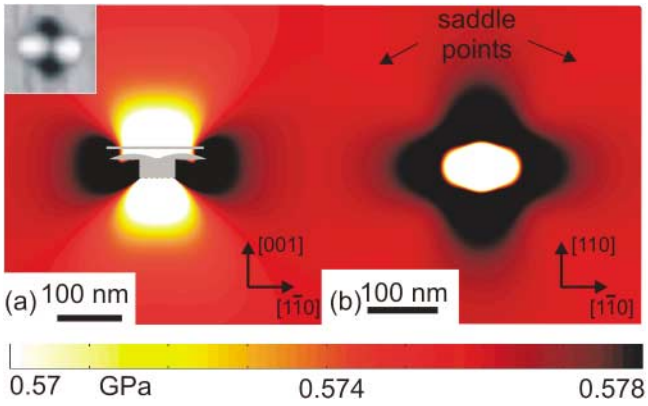

FIG. 2 (color). Strain energy density distribution generated by a buried QDM. (a) Cross-sectional view and (b) top view for a QDM capped with 13 nm GaAs. The main minimum directly above the molecule and the saddle points in the [100] and [010] directions are visible. The inset shows an AFM image of a typical QDM.

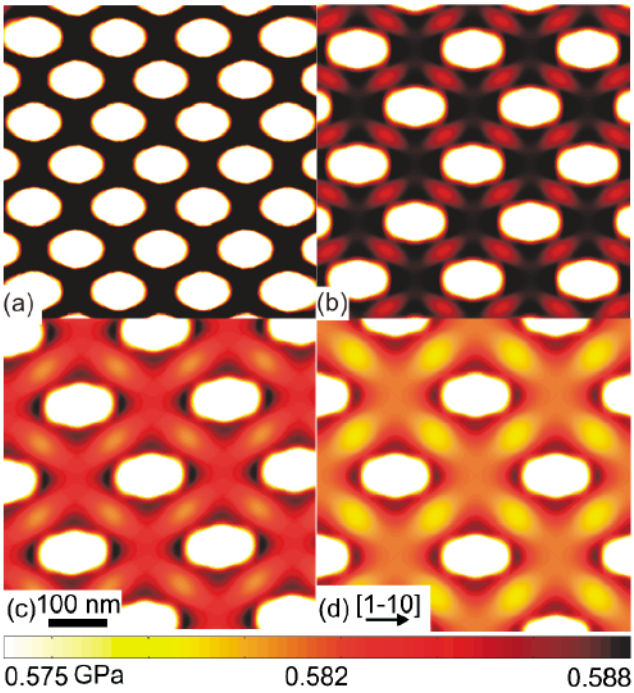

FIG. 3 (color). Simulation of the strain energy density distribution for arrays with (a) 103 nm, (b) 157 nm, (c) 179 nm, and (d) 200 nm periodicity. In (a) only the main minima are visible. If the periodicity is increased, elongated satellite minima develop between main minima.

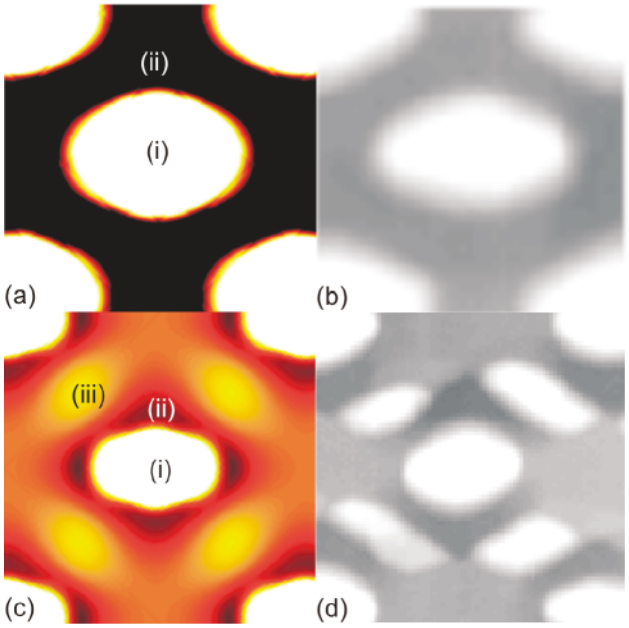

FIG. 4 (color). Comparison of theory and experiment. (a) and (b) compare the strain energy density simulation with the AFM results for the unit cell of a pattern with 103 nm periodicity and in (c) and (d) for 200 nm periodicity. All images are magnifications from Figs. 1 and 3. Three different areas are identified: (i) low strain energy density in the main minimum, (ii) an area with higher strain energy density, and (iii) satellite minima. The corresponding areas in (b),(d) are the vertically aligned QD, a depression area around the vertically aligned QD and the satellite QD in (d).

four saddle points, which appear 120 nm away from the center of the QDM.

In Fig. 3(a) the E_{str} distribution for an array of QDMs with a periodicity of 103 nm is shown. For this periodicity the main E_{str} minima coincide with the saddle point of the neighboring QDM. Satellite minima therefore do not occur as separate features in the E_{str} distribution. If the periodicity increases [Figs. 3(b)–3(d)], the saddle points of the two neighboring QDMs start to interfere constructively and the satellite minima become increasingly more pronounced on the GaAs surface. Similar to Fig. 2, elongated E_{str} maxima which point to the [110] and [1$\bar{1}$0] directions occur next to the main E_{str} minima.

Epitaxial growth is driven by the chemical potential distribution on a substrate surface, which (for a flat surface) is proportional to the E_{str} distribution [3]. We therefore expect InGaAs material to accumulate in areas of minimum E_{str}, and to avoid areas of maximum E_{str}.

Figure 4 shows a magnification of both the simulation of the E_{str} distribution as well as the AFM images of the stacked InGaAs layer for a pattern periodicity of 103 and 200 nm. For the small periodicity in Fig. 4(a), the simulation shows (i) pronounced main E_{str} minima and (ii) an area with high E_{str}. Comparing with the AFM experiment in Fig. 4(b) it is evident that the InGaAs QD forms on the area of minimum E_{str}. Also the shape of the QD base corresponds to the shape of the E_{str} minimum. Both features are elongated into the [1$\bar{1}$0] direction, which is a result of the strain-field superposition of the two QDs forming the buried QDM. The correlation between the shape of a strain field and the shape of a QD grown on this strain field has already been pointed out in [6]. From Figs. 4(a) and 4(b) we conclude that the InGaAs layer probes the E_{str} distribution created by the buried QDM layer. More detailed features are found for the 200 nm periodicity sample in Figs. 4(c) and 4(d). In this case InGaAs material accumulates not only on the main minimum [labeled (i)] but also on the satellite E_{str} minima [labeled (iii)].

The simulation is capable to predict the position, base size, and shape as well as the lateral orientation of the satellite QDs with reasonable precision. Other features are the four E_{str} maxima [labeled (ii)] next to the main minimum in the [110] and [1$\bar{1}$0] directions. In the AFM image this characteristic is accentuated in the [110] direction as shallow triangular depressions, which implies that the InGaAs material avoids areas on the surface, which experience a high E_{str}. Shallow depressions at positions of E_{str} maxima pointing into the [1$\bar{1}$0] direction can be found at various QDs in Fig. 2.

To investigate the origin of the satellite E_{str} minima in the array simulation, we performed a second set of

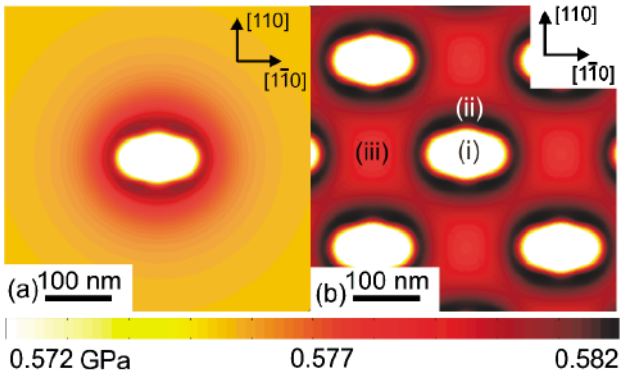

FIG. 5 (color). Simulation without anisotropy. (a) The strain energy density simulation of the same QDM as in Fig. 2(b). Here the anisotropic contribution is neglected resulting in an elliptical strain energy density distribution. In (b) we calculate the same array as in Fig. 3(d). We observe (i) the main strain energy density and (ii) areas with higher strain. (iii) Minima develop between the second nearest neighbors in the [1$\bar{1}$0] directions.

simulations, in which we switched off the anisotropy of the GaAs crystal. A similar theoretical investigation has been presented in Ref. [17]. Figure 5(a) shows the E_{str} distribution for the same buried QDM as in Fig. 2(b). Without anisotropy, the elliptic E_{str} distribution lacks the pronounced maxima in the [110] and [1$\bar{1}$0] directions and no saddle points are observed. Figure 5(b) displays the E_{str} distribution of an array of QDM analog to Fig. 3(d) with a periodicity of 200 nm. We observe (i) the main minimum, responsible for the vertical alignment, and (ii) the areas of higher E_{str} around the QDM. In contrast to Fig. 3 we observe (iii) E_{str} minima between the second nearest neighbors along the [1$\bar{1}$0] direction, which clearly contradicts the formation of satellite QDs between two nearest next neighbors as observed in the experiment. The comparison between Figs. 3 and 5 demonstrates that the E_{str} minima between the nearest next neighbors can be explained only if the crystal anisotropy is taken into account.

In conclusion, the ability to fabricate highly ordered arrays of self-assembled quantum dots with different periodicities opens the door to study novel growth phenomena that are caused by strain-field interferences. Such growth phenomena include the formation of QDs on satellite E_{str} minima and the formation of shallow depressions in areas of highest strain. The good agreement between measured morphology and calculated E_{str} distribution implies that, in the future, a relatively simple calculation of the E_{str} distribution can help to predict the position, size, and shape of QDs in two- and three-dimensional periodic QD crystals. Furthermore, we showed that taking the anisotropy of GaAs into account is essential for simulations of strain fields in this material system.

The authors thank U. Waizmann, T. Reindl, and M. Riek for their help in sample preparation, R. Songmuang and C. Deneke for fruitful discussions, and K. v. Klitzing for continuous support and interest. The work was supported by the BMBF (01BM906/4).

*Electronic address: H.Heidemeyer@fkf.mpg.de

[1] J. Y. Yao, T. G. Andersson, and G. L. Dunlop, J. Appl. Phys. **69**, 2224 (1991).
[2] T. S. Kuan and S. S. Iyer, Appl. Phys. Lett. **59**, 2242 (1991).
[3] Q. Xie, A. Madhukar, P. Chen, and N. P. Kobayashi, Phys. Rev. Lett. **75**, 2542 (1995).
[4] G. S. Solomon, J. A. Trezza, A. F. Marshall, and J. S. Harris, Jr., Phys. Rev. Lett. **76**, 952 (1996).
[5] J. Tersoff, C. Teichert, and M. G. Lagally, Phys. Rev. Lett. **76**, 1675 (1996).
[6] F. Liu, S. E. Davenport, H. M. Evans, and M. G. Lagally, Phys. Rev. Lett. **82**, 2528 (1999).
[7] Q. X. Pei, C. Lu, and Y. Y. Wang, J. Appl. Phys. **93**, 1487 (2003).
[8] O. G. Schmidt, N. Y. Jin-Phillipp, C. Lange, U. Denker, K. Eberl, R. Schreiner, H. Gräbeldinger, and H. Schweizer, Appl. Phys. Lett. **77**, 4139 (2000).
[9] H. Lee, J. A. Johnson, J. S. Speck, and P. M. Petroff, J. Vac. Sci. Technol. B **18**, 2193 (2000).
[10] Y. Nakamura, O. G. Schmidt, N. Y. Jin-Phillipp, S. Kiravittaya, C. Müller, K. Eberl, H. Gräbeldinger, and H. Schweizer, J. Cryst. Growth **242**, 339 (2002).
[11] O. G. Schmidt, C. Deneke, S. Kiravittaya, R. Songmuang, H. Heidemeyer, Y. Nakamura, R. Zapf-Gottwick, C. Müller, and N. Y. Jin-Phillipp, IEEE J. Sel. Top. Quantum Electron. **8**, 1025 (2002).
[12] R. Hey, M. Wassermeier, M. Höricke, E. Wiebicke, and H. Kostial, J. Cryst. Growth **201/202**, 582 (1999).
[13] V. Holý, G. Springholz, M. Pinczolits, and G. Bauer, Phys. Rev. Lett. **83**, 356 (1999); G. S. Solomon, S. Komarov, and J. S. Harris, Jr., J. Cryst. Growth **201/202**, 1190 (1999).
[14] D. A. Faux and G. S. Pearson, Phys. Rev. B **62**, 4798 (2000).
[15] M. Meixner, E. Schöll, M. Schmidbauer, H. Raidt, and R. Köhler, Phys. Rev. B **64**, 245307 (2001).
[16] Y. A. Burenkov, S. Y. Davydov, and S. P. Nikanorov, Sov. Phys. Solid State **17**, 1446 (1975).
[17] V. Holý, J. Stangl, S. Zerlauth, G. Bauer, N. Darowski, D. Lübbert, and U. Pietsch, J. Phys. D **32**, A234 (1999).